Chinese Chemical Letters 31 (2020) 2295–2299

Contents lists available at ScienceDirect

Chinese Chemical Letters

journal homepage: www.elsevier.com/locate/cclet

Communication

Metal-organic framework derived Co_3O_4/PPy bifunctional electrocatalysts for efficient overall water splitting

Yongli Tong[a,b], Hengqi Liu[a], Meizhen Dai[a], Li Xiao[a,*], Xiang Wu[a,*]

[a] School of Materials Science and Engineering, Shenyang University of Technology, Shenyang 110870, China
[b] School of Science, Shenyang Ligong University, Shenyang 110159, China

ARTICLE INFO

Article history:
Received 17 December 2019
Received in revised form 5 February 2020
Accepted 10 March 2020
Available online 10 June 2020

Keywords:
Metal-organic framework
Co_3O_4/PPy
Bi-functionality
Electrocatalyst
OER and HER

ABSTRACT

In this work, we report Co_3O_4@PPy hybrid structured electrode materials for overall water splitting. The as-synthesized Co_3O_4/PPy-120 samples present excellent electrocatalytic performances for OER and HER and long durability. It only requires an operating potential of 1.67 V to deliver a current density of 10 mA/cm^2 with a remarkable durability for 28 h. The superior electrocatalytic performances mainly can be attributed to the unique heterostructures and the synergistic effects between PPy and Co_3O_4 electrode materials.

Due to worldwide overconsumption of fossil fuels, it is necessary to find environmental-friendly and renewable energy materials [1–3]. Hydrogen is recognized as one of the most promising green energy owing to its rich reservation on the earth [4,5]. However, the efficiency of overall water splitting for harvesting of hydrogen largely lowers due to the kinetically sluggish OER. Thus, developing highly active and cost-effective catalysts is very essential to improve the energy conversion efficiency [6,7]. Currently, some noble metals such as RuO_2/IrO_2 and Pt exhibit outstanding catalytic performances for OER and HER. However, the high cost and scarcity hinder their further applications. Therefore, much attention has been focused on alternative earth-abundant and inexpensive non-noble metals materials. Nevertheless, only a few catalyst materials possess the abilities to catalyze both HER and OER. Therefore, the development of bi-functional catalytic materials is a challenge in overall water splitting.

Metal-organic frameworks (MOFs), which are formed by linking inorganic ions and organic chains through strong coordination bonds, have been concerned owing to their unique structures and intrinsically large surface area. MOFs present multi-functionalities for supercapacitors [8], lithium ion batteries [9], gas adsorption/separation [10] and heterogeneous catalysis [11]. Moreover, MOFs can be transformed into metal oxides, porous carbons, carbon/metal and metal sulfides through postsynthesis treatment. Among them, Co-based derivatives (Co_3O_4) have attracted considerable attentions as water splitting catalysts due to their thermal stability, abundant reserves and environmental friendliness in alkaline electrolytes [12,13]. However, MOF derivatives are mostly in powder form, where the usage of adhesives takes many disadvantages in catalytic performances. Meanwhile, it is challenging to synthesize them with controllable morphologies though MOFs precursors. Conducting polymers, such as PPy and PANI, usually combine with other transition metal compounds owing to their intrinsic high conductivity, facile preparation and superior environmental stability [14,15].

In this work, Co-based MOFs are synthesized by a facile approach on Ni foam substrate, and transformed to Co_3O_4 nanoleaves through thermal pyrolysis. Finally, Co_3O_4 nanoleaves are decorated using polypyrrole through an electrodeposition method. The hybrid Co_3O_4/PPy nanostructures exhibit remarkable electrocatalytic performances for OER and HER with low overpotential as well as remarkable durability. It might result from their enhanced conductivity and synergistic effect between Co_3O_4 and PPy samples.

Prior to experiment, a piece of Ni foam was treated by 1 mol/L HCl solution to remove surface impurity, and then washed ultrasonically with deionized water and absolute ethanol several times, respectively. All other chemicals were used without any further purification.

The details of procedure are shown as follows. 0.06 mol/L of $Co(NO_3)_2{\cdot}6H_2O$ and 0.3 mol/L of 2-methylimidazole (Hmim)

* Corresponding authors.
E-mail addresses: xiao.li@sut.edu.cn (L. Xiao), wuxiang05@sut.edu.cn (X. Wu).

https://doi.org/10.1016/j.cclet.2020.03.029

powder were dissolved in 50 mL deionized water separately with magnetic stirring for 30 min at room temperature. Subsequently, $Co(NO_3)_2{\cdot}6H_2O$ pink solution was added into the Hmim solution quickly and the pretreated nickel foam (4×4 cm^2) was completely immersed in the above solution for 2 h. Then the sample supported on nickel foam was rinsed with deionized water and absolute ethanol several times and dried overnight at 60 °C in an oven. Finally, the Co-MOF precursor was annealed at 300 °C for 1 h at a ramping rate of 1 °C/min in muffle furnace to obtain Co_3O_4 nanoleaves.

Composites were fabricated through a chronopotentiometry deposition method. To prepare polypyrrole, 1 g p-TSA was dissolved in 60 mL deionized water and stirred for 15 min. Then 0.2 mL pyrrole was dropped into the above solution slowly and stirred for 30 min to obtain clear solution. The above mentioned Co_3O_4 products were used as working electrode. Pt foil and Ag/AgCl electrode was acted as the counter and reference electrodes, respectively. The potential window is 0.95 V. After electrodeposition, Co_3O_4/PPy product was rinsed several times with deionized water and ethanol, and dried at 60 °C for 8 h.

The phase purity and crystal structure of the as-fabricated products were analyzed by power X-ray diffraction analyzer (XRD, 7000, Shimadzu). Fourier transform infrared spectrum (FTIR, 4000–500 cm^{-1}) and X-ray photoelectron spectroscopy (XPS, ESCALAB 250 Xi, Thermo Scientific) were used to study the composition of the as-prepared samples. The morphology of the product were characterized by scanning electron microscopy (SEM, Gemini 300-71- 31).

Electrochemical measurements of the as-synthesized samples were studied using a CHI660E electrochemical workstation (Chenhua, Shanghai) in a typical three-electrode system. The as-prepared samples were used as working electrode, Ag/AgCl electrode and graphite rod as reference electrode and counter electrode, respectively. OER and HER performances were investigated in 1.0 mol/L KOH solution (pH 13.7). The measured potentials were converted to the reversible hydrogen electrode (RHE) according to Nernst equation: $E_{RHE} = E_{SCE} + 0.198 + 0.059 \times$ pH, where E_{SCE} refers the measured potentials.

The overpotential (η) could be obtained through the equation: $\eta = E_{RHE} - 1.23$. To evaluate the performances of OER and HER, linear sweep voltammetry (LSV) polarization curves were measured at a scan rate of 2 mV/s. ECSA values of OER and HER were calculated *via* cyclic voltammetry (CV) curves in the non-faradaic voltage range. The potential range of OER is from 0.1 V to 0.2 V and that of HER is from -0.3 V to -0.2 V. As scan rates increases (10−50 mV/s), current density changes linearly. The slope of the line is considered twice of C_{dl}. Electrochemical impedance spectroscopy (EIS) curves were recorded in the same electrolyte ranging from 10^{-1} Hz to 10^5 Hz at 5 mV.

X-ray diffraction (XRD) patterns are used to analyze the crystal structures of the as-prepared samples (Fig. 1a). The characteristic peaks of black curve at 44.6°, 52.0° and 76.6° belong to nickel foam (JCPDS No. 42-0712). The others at 2θ values of 31.3°, 36.9°, 59.4°, 65.2° are in accordance with (220), (311), (511) and (440) crystal planes of Co_3O_4 products (JCPDS No. 42-1467). It is confirmed that Co-MOF precursor is converted into Co_3O_4 products through thermal pyrolysis. It could be observed that the intensities of all the diffraction peaks in the red curve are obviously weakened, which indicates that Co_3O_4 products are successfully coated by polypyrrole. FTIR spectrum is used to further identify it, as shown in Fig. 1b. The absorption peak located at 1095 cm^{-1} can be ascribed to N—H and C—H vibration modes in pyrrole rings. The peaks at 1637 cm^{-1} and 3331 cm^{-1} correspond to the vibration mode of absorbing water. The peaks at 2859 cm^{-1} and 2930 cm^{-1} are thought to be N—H bond of aromatic amines [16].

XPS measurements are also conducted to analyze surface composition of samples. The full spectra show Co, O, Ni and N

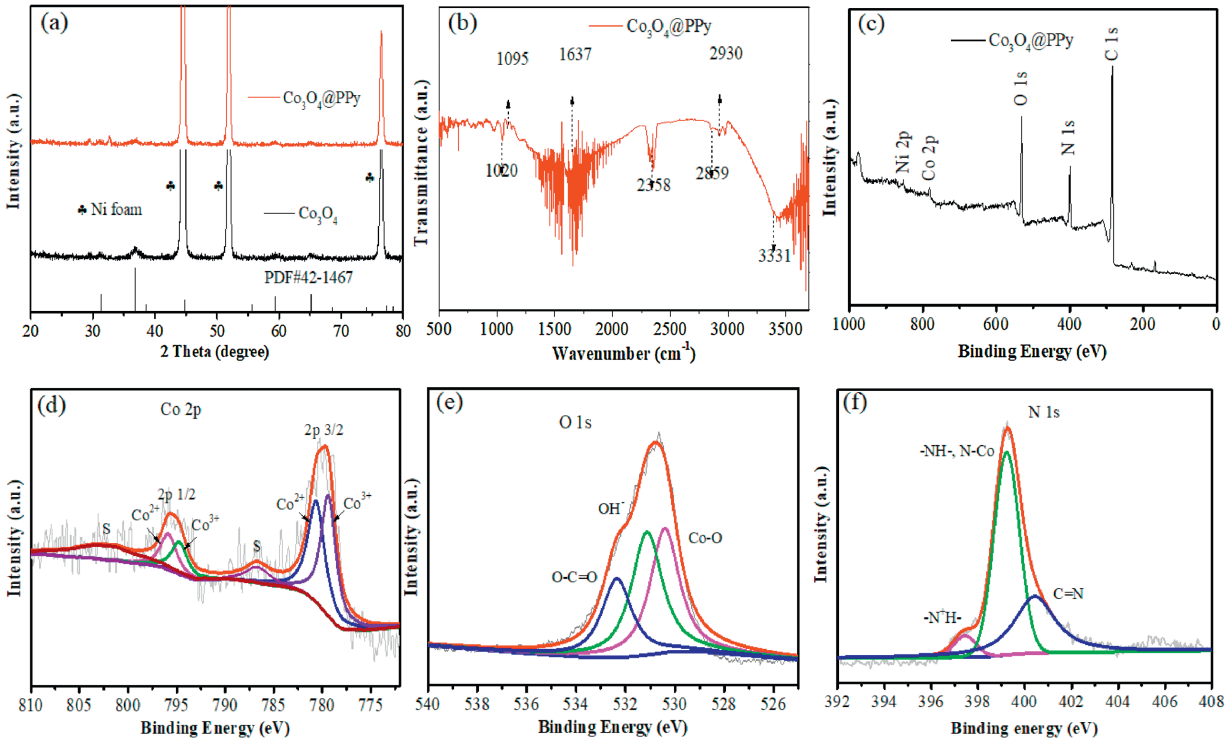

Fig. 1. Chemical composition characterization (a) XRD patterns of Co_3O_4 nanoleaves and Co_3O_4/PPy-120. (b) FTIR of Co_3O_4/PPy-120. (c) Full spectrum, (d) Co 2p, (e) O 1s and (f) N 1s XPS spectra of the Co_3O_4/PPy-120.

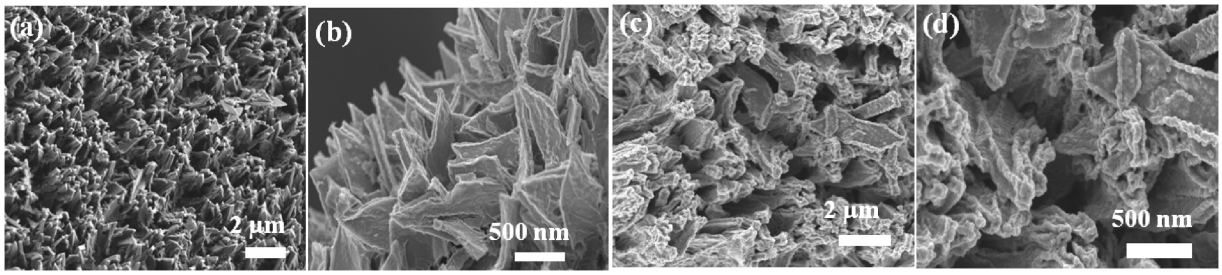

Fig. 2. Morphology characterization: (a, b) SEM images of Co_3O_4 nanoleaves. (c, d) SEM images of the Co_3O_4/PPy-120.

elements in Fig. 1c, which is consistent with XRD and FTIR analysis. Fig. 1d is the high-resolution XPS spectrum of Co element. It shows two strong peaks of Co $2p_{1/2}$ and Co $2p_{2/3}$ and two satellite peaks which result from spin-orbital coupling of Co $2p_{1/2}$ and Co $2p_{3/2}$ orbits. The energy interval between strong peaks at 795.3 eV and 779.8 eV is about 15.5 eV, which is the characteristic of Co $2p_{1/2}$ and Co $2p_{3/2}$ orbits of Co_3O_4 phase. The peaks show slightly shift compared with those of pure Co_3O_4 samples [17], indicating electron transfer and strong interaction between Co_3O_4 and PPy samples. The fitting peaks at 795.8 and 780.7 eV are assigned to Co^{2+}, and the peaks at 794.8 and 779.3 eV could be ascribed to Co^{3+}. The main peak in the O 1s region is divided into three peaks at 530.4, 531.1 and 532.3 eV (Fig. 1e), which are associated with oxygen in Co_3O_4, hydroxide groups and surface lattice oxygen, respectively. Three peaks are separated in the deconvolution of the N 1s region centered at 397.9, 399.4 and 400.3 eV, which correspond to the C=N defects of PPy, the —NH— segment in PPy backbone and the connections of N—Co between PPy and Co_3O_4, respectively (Fig. 1f) [18].

The morphologies of the as-synthesized samples are observed through SEM. Fig. 2a shows that Co_3O_4 samples are uniformly grown on nickel foam with a leaf-like two-dimensional shape. Through further observation (Fig. 2b), it can be clearly found that the width of each nanoleaf is approximately 400 nm with an average thickness of 20 nm. Figs. 2c and d exhibit that Co_3O_4 samples are uniformly covered by a layer of thin film, indicating that PPy was successfully deposited due to coordinating between cobalt ions and -NH- sections in polypyrrole chains. Co_3O_4 nanoleaves cannot be seen clearly, revealing a strong interaction between PPy and Co_3O_4 nanoleaves.

The OER catalytic activities of Co_3O_4/PPy samples are studied by LSV polarization curves. A small hump before catalytic reaction corresponds to redox peak of Co_3O_4 at 1.1–1.2 V, in which the valence state of cobalt ions ranges from Co^{2+}/Co^{3+} to Co^{3+}/Co^{4+} as shown in Fig. 3a. Those active sites facilitate OH^- absorption for OER in alkaline solution. In addition, the contacting with electrolyte plays an important role for OER. In order to optimize the performances of catalysts, the samples by 30 s electrodepositing PPy on Co_3O_4 products are denoted as Co_3O_4/PPy-30 and 120 s (Co_3O_4/PPy-120) and 240 s (Co_3O_4/PPy-240), respectively. As shown in Fig. 3b, Co_3O_4/PPy-120 shows the overpotential of 220 mV at 10 mV/s, which is lower than Co_3O_4/PPy-30 (260 mV), Co_3O_4/PPy-240 (280 mV) and pure Co_3O_4 (320 mV). As expected, Co_3O_4/PPy-120 shows the best catalytic performance with an overpotential of 310 mV at 100 mV/s in comparison to the other three materials. The overpotentials are comparable to those of cobalt-based catalysts [19–22].

Tafel plots are used to analyze OER kinetics from polarization curves (Fig. 3c). Co_3O_4/PPy-120 samples present a Tafel slope of 57.7 mV/dec, which is smaller than Co_3O_4/PPy-30 (89.8 mV/dec),

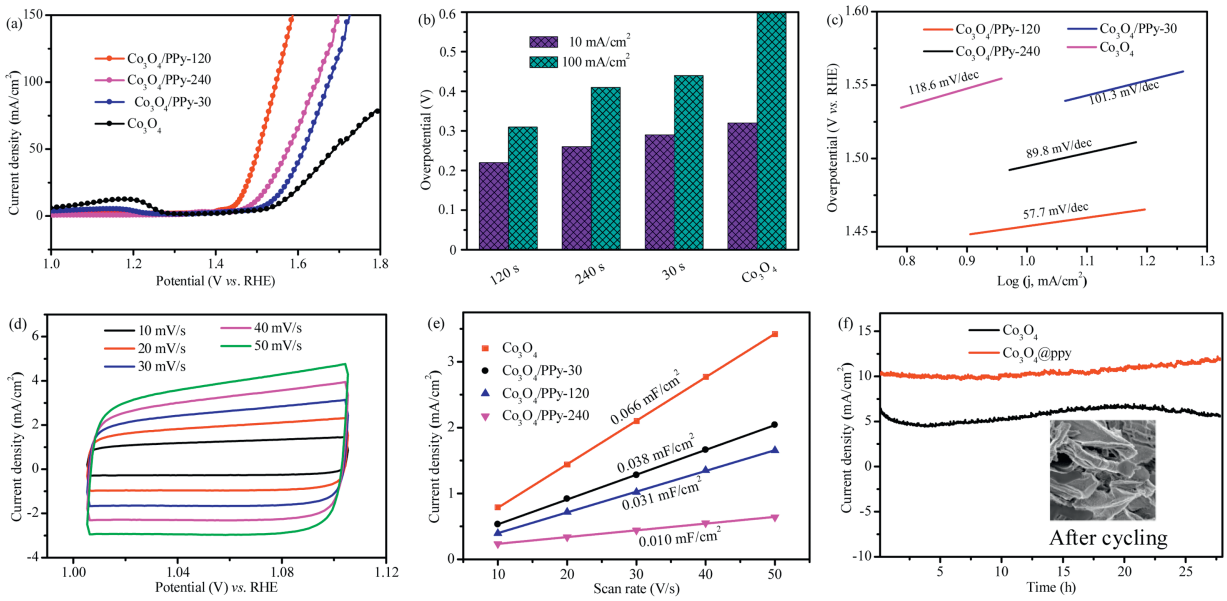

Fig. 3. OER electrocatalytic performances: (a) LSV curves. (b) Overpotential at 10 and 100 mA/cm^2. (c) Tafel plot. (d) CV curves. (e) ECSA analysis. (f) Chronoamperometric plot.

Co_3O_4/PPy-240 (101.3 mV/dec) and pure Co_3O_4 (118.6 mV/dec). These results reveal that the introduction of PPy can accelerate electrons transferring to the electrode surface due to its superior conductivity, resulting in great improvement of catalytic kinetic.

Fig. 3d shows CV curves of Co_3O_4/PPy-120 samples between 1.0 V and 1.1 V in non-Faradaic region. It can be clearly found that no visible redox peaks appear, indicating a double layer capacitive behavior. The double-layer capacitance (C_{dl}) is proportional to the electrochemical surface area (ECSA) [23]. As shown in Fig. 3e, the C_{dl} of Co_3O_4/PPy-120 is 0.031 mF/cm^2, while those of pure Co_3O_4, Co_3O_4/PPy-30 and Co_3O_4/PPy-240 are 0.066 mF/cm^2, 0.038 mF/cm^2 and 0.010 mF/cm^2, respectively. ECSA of Co_3O_4/PPy-120 sample is not highest in these samples. It shows that the intrinsic synergistic effect between Co_3O_4 and PPy results in a low overpotential.

To assess durability and stability of the as-prepared samples, the long-term cycling of Co_3O_4/PPy-120 is tested at a current density of 10 mA/cm^2 for 28 h. Fig. 3f shows the curve of Co_3O_4/PPy-120 is smoother than that of bare Co_3O_4 nanoleaves. Moreover, this curve does not decline almost even after 28 h, suggesting its excellent durability, which could be also confirmed through the inset in Fig. 3f. The morphology of Co_3O_4/PPy-120 almost not changes with negligible collapse and aggregation after 28 h cycling. The above results show the amorphous PPy film can effectively prevent Co_3O_4 from collapsing due to volume changing repeatedly in OER process.

The HER electrocatalytic activities of the as-prepared samples were also investigated in the same electrolyte condition. Similar to OER, Figs. 4a and b show Co_3O_4/PPy-120 samples with an overpotential of 140 mV to deliver a current density of 10 mA/cm^2, which is lower than those of Co_3O_4/PPy-240 (175 mV), Co_3O_4/PPy-30 (214 mV) and Co_3O_4 nanoleaves (260 mV). The values of overpotential are comparable to those of cobalt-based catalysts reported recently [19,24,25].

In addition, Co_3O_4/PPy-120 samples possess favorable HER kinetics with a lower Tafel slope of 83 mV/dec compared to Co_3O_4/PPy-240 (95 mV), Co_3O_4/PPy-30 (141 mV) and Co_3O_4 nanoleaves (115 mV). The lower Tafel slope shows an operative Volmer-Heyrovsky reaction pathway. Typically, in alkaline solution, HER reaction mechanisms can be described through the following three steps [26]:

$$H_2O + e^- \rightarrow H_{ads} + OH^- \text{ (Volmer)} \quad (1)$$

$$H_2O + e^- + H_{ads} \rightarrow H_2 + OH^- \text{ (Heyrovsky)} \quad (2)$$

$$H_{ads} + H_{ads} \rightarrow H_2 \text{ (Tafel)} \quad (3)$$

The OH^- ions by water splitting might be prone to chemisorbing on Co_3O_4 sites at Co_3O_4/PPy interface due to strong electrostatic force with positive Co^{2+}/Co^{3+} ions. While PPy sites could promote H chemisorptions, which corresponds to Volmer process [27,28]. It can also make hydrogen-metal binding energy to a relatively appropriate level, and facilitate desorption/release of H_{ads} from active sites.

The EIS measurements of Co_3O_4/PPy-120 and Co_3O_4 samples are also carried out to investigate the kinetics performance in alkaline conditions (Fig. 4c). The slope of the straight part in Co_3O_4/PPy-120 samples is close to that of vertical part, revealing its small electrocatalytic resistance. And its slope is larger than that of Co_3O_4 nanoleaves, indicating a reduced electrocatalytic resistance owing to the introduction of PPy. Moreover, it could be observed that a short semicircle with a small charge transfer resistance (R_{ct}) in inset, further proving its fast electron transfer process [29,30]. The above results reveal that HER kinetics of electrodes are greatly promoted after covering of a layer of amorphous PPy, which shortens electrons diffusion/transfer paths due to the synergistic effects between PPy and Co_3O_4 materials. Fig. 4d shows EIS of two electrode materials. It demonstrates low resistance of the composite.

The ECSA of the as-prepared samples in HER is calculated according to the same method as OER. As shown in Fig. 4e, The ECSA of Co_3O_4/PPy-120 samples is 0.0046 mF/cm^2, while the ones of Co_3O_4 nanoleaves, Co_3O_4/PPy-30, Co_3O_4/PPy-240 are 0.0054, 0.0042 and 0.0025 m;F/cm^2, respectively. Durability is very important to assess HER catalytic performance of electrodes. In the first 4 h, the curve drops a lot (about 23 % loss), and then nearly

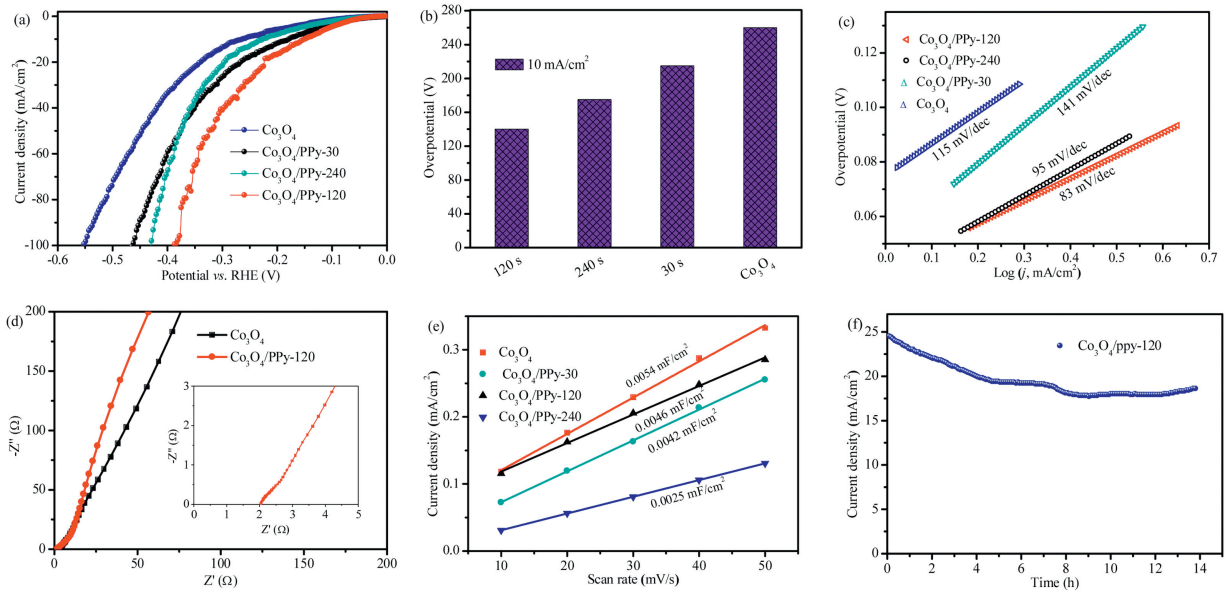

Fig. 4. HER electrocatalitic performances: (a) LSV curves. (b) The overpotential at 10 mA/cm^2. (c) Tafel plot. (d) Nyquist plots. (e) ECSA analysis. (f) Chronoamperometric plot.

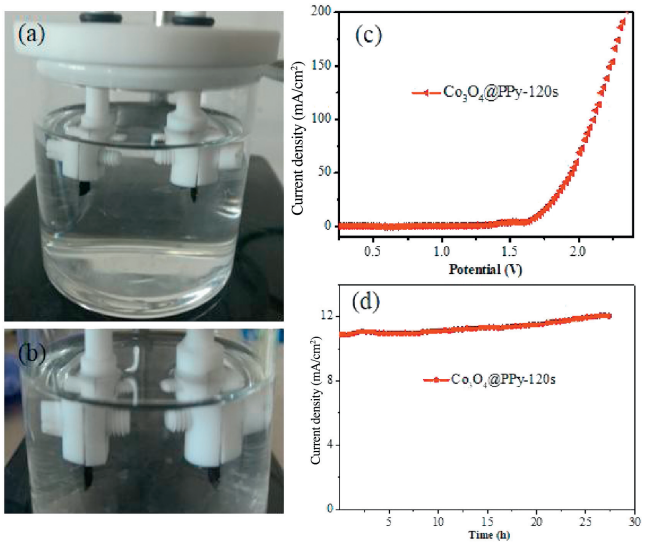

Fig. 5. Overall water splitting of the Co_3O_4/PPy-120: (a, b) Photograph of two-electrode configuration. (c) Polarization curves. (d) Chronoamperometric plot.

remains stable with negligible loss, suggesting its superior stability as shown in Fig. 4f.

In view of excellent OER and HER catalytic activities of Co_3O_4/PPy-120 samples, their overall water splitting performances are investigated in two-electrode configuration in 1 mol/L alkaline solution. The device is shown in Figs. 5a and b. It can be observed that some bubbles appear from the surface of working electrodes. It shows a catalytic activity with a cell voltage of 1.67 V at 10 mA/cm^2, which is only 0.10 V higher than the benchmark Pt/C||RuO_2 electrodes. Long-term stability of Co_3O_4/PPy-120 electrode is tested in 1 mol/L KOH at 0.58 V potential in Fig. 5d. After 28 h, the current density remains basically constant, indicating superior stability of water splitting.

In summary, Co_3O_4/PPy products are fabricated on nickel foam by a facile method. The depositing time of PPy seriously affect catalytic performances of the electrodes. Co_3O_4/PPy-120 samples possess superior OER and HER electrocatalytic performance with a low overpotential and remarkable durability. Meanwhile, water electrolyzer exhibits an excellent performance, which mainly benefit from the unique structures and synergistic effect between Co_3O_4 and PPy materials. The introduction of PPy improves the conductivity of electrodes and facilitates the electronic transfer during OER and HER.

Declaration of competing interest

The authors declare that they have no known competing financial interests or personal relationships that could have appeared to influence the work reported in this paper.

Acknowledgments

This project is supported by the Opening Project of State Key Laboratory of Advanced Technology for Materials Synthesis and Processing (Wuhan University of Technology) (No. 2020-KF-12).

References

[1] S.J. Guo, Y. Yu, Q. Zhang, Chin. Chem. Lett. 28 (2017) 2169–2170.
[2] D. Zhao, H. Liu, X. Wu, Nano Energy 57 (2019) 363–370.
[3] H. Liu, D. Zhao, P. Hu, et al., Chem. Eng. J. 373 (2019) 485–492.
[4] X. Du, X. Zhang, Int. J. Hydrogen Energy 44 (2019) 24705–24711.
[5] W.Q. Yang, J.R. Zeng, Y.X. Hua, et al., J. Power Sources 436 (2019) 226887.
[6] Y.Q. Feng, H.Y. Cheng, J. Han, et al., Chin. Chem. Lett. 28 (2017) 2254–2258.
[7] M. Li, Y. Zhu, H. Wang, et al., Adv. Energy Mater. 9 (2019) 1803185.
[8] K. Wang, H. Wang, R. Bi, et al., Inorg. Chem. Front. 6 (2019) 2873–2884.
[9] X. Yang, Y. Wang, Y. Hu, et al., ChemElectroChem. 6 (2019) 3657–3666.
[10] M. Mofarahi, F. Gholipour, Microporous Mesoporous Mater. 200 (2014) 1–10.
[11] Y.L. Tong, D.L. Qi, B.Q. Chi, W.Q. Zhang, Sci. Adv. Mater. 11 (2019) 338–344.
[12] K. Shrestha, S.H. Lee, H. Ahn, S.H. Han, Microporous Mesoporous Mater. 153 (2012) 163–165.
[13] M. Ding, J. Zhou, H. Yang, et al., Chin. Chem. Lett. 31 (2020) 71–76.
[14] S.H. Ye, G.R. Li, Front. Chem. Sci. Eng. 12 (2018) 473–480.
[15] Y. Xu, D. Guo, T. Li, et al., J. Colloid Interfaces. Sci. 565 (2020) 23–34.
[16] J.L. Liu, W.W. Zhou, L.F. Lai, et al., Nano Energy 2 (2013) 726–732.
[17] J. Feng, W. Song, L. Sun, L. Xu, RSC Adv. 6 (2016) 110337–110343.
[18] S. Bao, S. Luo, S. Yan, et al., Electrochim. Acta 307 (2019) 293–301.
[19] X. Wei, Y.H. Zhang, H.C. He, et al., Chem. Commun. 55 (2019) 6515.
[20] H. Mao, X. Guo, Y.L. Fu, et al., Appl. Surf. Sci. 485 (2019) 554–563.
[21] J.K. Zhu, W.M. Tu, Z.Y. Bai, et al., Electrochim. Acta 323 (2019) 134821.
[22] J. Shen, J. Gao, L.D. Ji, X.R. Chen, C. Wu, Appl. Surf. Sci. 497 (2019) 143818.
[23] D. Xiong, Q. Zhang, W. Li, et al., Nanoscale 9 (2017) 2711–2717.
[24] J. Yang, L. Wei, T. Zhao, et al., Electrochim. Acta 318 (2019) 949–956.
[25] D. Zhao, M. Dai, H. Liu, et al., Adv. Mater. Interfaces 6 (2019) 1901308.
[26] H. Liu, X. Ma, Y. Rao, et al., ACS Appl. Mater. Interfaces 10 (2018) 108907.
[27] H. Mao, X. Guo, Y. Fu, et al., Appl. Surf. Sci. 485 (2019) 554–563.
[28] Y.L. Tong, B.Q. Chi, D.L. Qi, X.Y. Liu, Sci. Adv. Mater. 11 (2019) 1087–1092.
[29] H. Liu, S. Luo, S. Yan, et al., J. Electroanal. Chem. 850 (2019) 113434.
[30] J. Li, S. Luo, X. Ding, et al., ACS Appl. Mater. Interfaces 10 (2018) 10786–10795.